Biophysical Journal, Volume *114*

Supplemental Information

Quantitative Characterization of Metastability and Heterogeneity of Amyloid Aggregates

Timir Baran Sil, Bankanidhi Sahoo, Subhas Chandra Bera, and Kanchan Garai

Supplementary Information

Quantitative Characterization of Metastability and Heterogeneity of Amyloid Aggregates

Timir Baran Sil, Bankanidhi Sahoo, Subhas Chandra Bera and Kanchan Garai*

Tata Institute of Fundamental Research, Hyderabad, India

Characterization of aggregation of TMR-Aβ42

Kinetics of aggregation of TMR-Aβ42:

An aliquot (1 mL) of 1.3 μM of TMR-Aβ42 was aggregated in 20 mM phosphate containing 150 mM NaCl, 5 mM βMe and 1 mM EDTA, pH 7.4 at 37 ℃ with continuous stirring. Aggregation was monitored using TMR fluorescence continuously in a fluorometer (PTI). Excitation and emission monochromators were set at 550 nm and 585 nm, respectively. Time course of aggregation of TMR-Aβ42 presented in Figure S1A shows three distinct phases, oligomerization, intermediate or 'lag' and fibril growth phase. It may be seen that the kinetic data presented here are similar to the data reported previously by Garai and Frieden (1).

Characterization of secondary structure of TMR-Aβ42 amyloids by circular dichroism (CD):

CD spectra of the monomeric and the aggregated TMR-Aβ42 prepared in 10 mM phosphate buffer were measured in a spectropolarimeter (Jasco). The aggregated TMR-Aβ sample was pelleted down by centrifugation at 16000×g, then the pellet was resuspended in 10 mM phosphate buffer, pH 7.4. Figure S1B shows a peak at 200 nm for the monomeric TMR-Aβ42 indicating random coil nature of the monomers. However, TMR-Aβ amyloids show a peak at 218 nm indicating β-sheet nature of the aggregates. Concentration of TMR-Aβ used in these measurements is 5 μM.

Atomic force microscopy (AFM) imaging of TMR-Aβ42 amyloids:

Morphology of aggregates was characterized by AFM (AFM Workshop, USA). Aggregated TMR-Aβ42 were placed on a freshly peeled layer of mica, incubated for 5 min and washed with deionized water. The sample was dried overnight at RT. The AFM was operated in the tapping mode. Figure S1C shows that TMR-Aβ42 form both long fibrillar structures and small globular aggregates. Taken together TMR-Aβ42 used here shows aggregation behavior similar to that were reported previously (1).

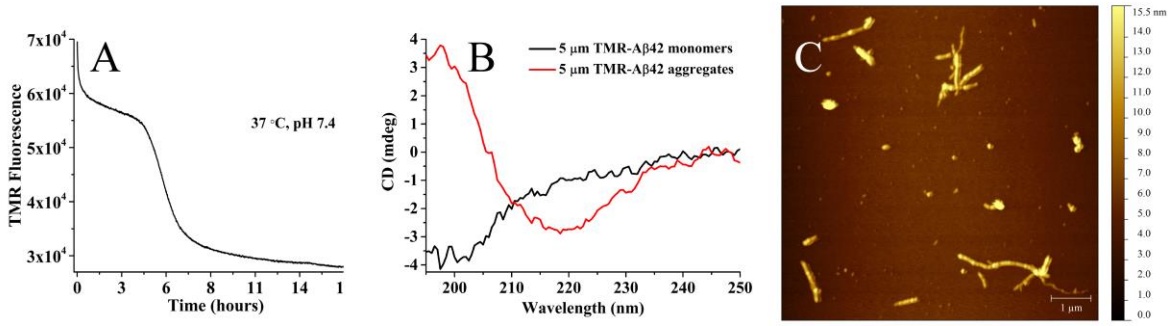

Figure S1. Characterization of aggregation of TMR-Aβ42. A) Kinetics of aggregation of TMR-Aβ42 monitored by TMR fluorescence. B) CD spectra of 5 μM TMR-Aβ42, soluble (black solid line) and aggregated (red solid line) in 10 mM phosphate buffer, pH 7.4 at 25 ℃. Clearly, TMR-Aβ aggregates are rich in β-sheet structures. C) Morphology of TMR-Aβ42 aggregates observed by AFM. Both, long fibrillar aggregates and small globular species can be observed in AFM.

Determination of hydrodynamic radii of the soluble TMR-Aβ42 using Fluorescence Correlation Spectroscopy (FCS)

Stock solution of monomeric TMR-Aβ42 was prepared by size exclusion chromatography purification using a Superdex peptide column (GE Healthcare) in 4 M GdnCl, containing 10 mM PBS (pH 7.4), 5 mM β-mercaptoethanol (βMe) and 1 mM EDTA. Only the monomeric fractions were collected to prepare the monomeric stock in 4 M GdnCl. The stock solution was diluted 200-fold to 25 nM final concentration in 0 or 4 M GdnCl containing 10 mM PBS with 5 mM β-Me, 1 mM EDTA, pH 7.4. FCS measurements were performed using a home built FCS set up. Hydrodynamic radii (R_h) were calculated from the measured diffusion times of free rhodamine B and TMR-Aβ (see equation 2 in the materials and methods section in the manuscript). The gray

and red bars in figure S2 represent R_h of the monomeric TMR-Aβ42 and the materials disaggregated from TMR-Aβ42 fibrils respectively. Clearly, R_h of the species formed upon disaggregation of fibrils are the same as the monomeric peptides at both 0 and 4 M GdnCl. These data indicate that in our disaggregation experiments TMR fluorescence arises from the monomeric peptides. Aggregated forms of TMR-Aβ42 have insignificant contribution to the fluorescence.

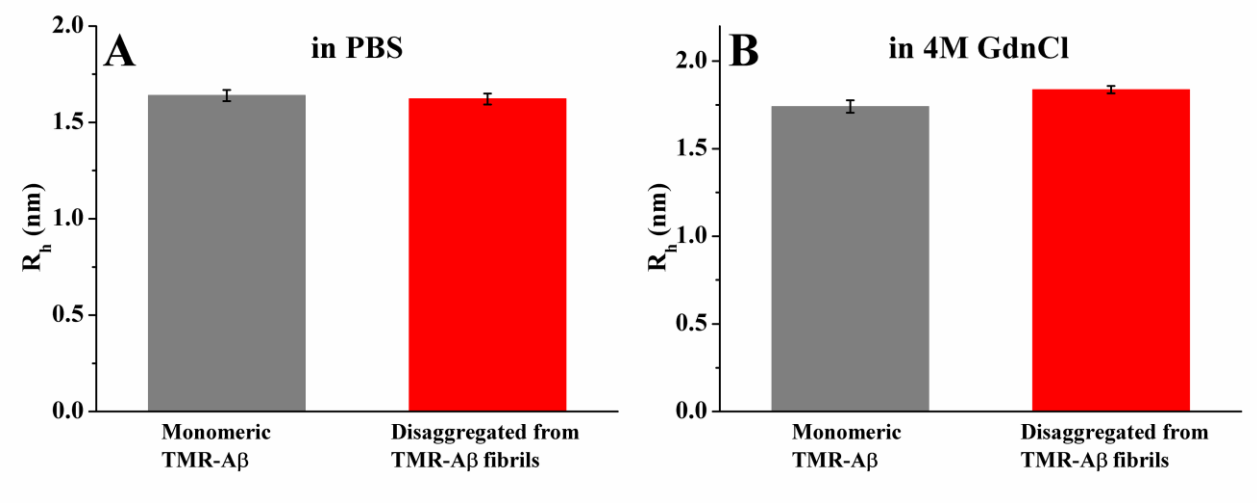

Figure S2. Hydrodynamic radii (R_h) of TMR-Aβ42 monomers (gray bars) and the peptides disaggregated from TMR-Aβ42 fibrils (red bars) in PBS (A) and in 4M GdnCl (B). Clearly, the disaggregated species have the same R_h as the monomeric peptide.

Relationship between $C_{soluble}$ and C_{total} for tyrosine at different concentrations of GdnCl

A 50 mg/ml stock tyrosine solution was prepared in 10 mM PBS buffer, pH 7.4. Tyrosine is poorly soluble in PBS hence the stock obtained was turbid. This stock was vortexed to mix thoroughly, then diluted immediately to 0.3, 0.6, 1.2, 2.4 and 4.8 mg/ml final concentration in 1.1, 3.2 and 5.3 M GdnCl. These solutions were kept at room temperature for 4 h and then centrifuged at 16000×g. The supernatants were separated carefully. Absorbance of the supernatants were measured using a spectrophotometer (Jasco). Supernatants were diluted appropriately prior to the measurements of absorbance to avoid artifacts that may arise due to inner filter effects at high concentrations of tyrosine. Soluble concentration of tyrosine was calculated using absorbance

value at 275 nm using extinction coefficient ε = 1440 $mol^{-1}cm^{-1}$. Figure S3 shows the plots of soluble concentration ($C_{soluble}$) versus total concentration (C_{total}) of tyrosine at various concentrations of GdnCl. It may be seen that these plots can be divided into two distinct regions: for $C_{total} < C_{sat}$, $C_{soluble} = C_{total}$ and for $C_{total} > C_{sat}$, $C_{soluble} = C_{sat}$ where the C_{sat} refers to saturation concentration. The C_{sat} of tyrosine are 0.7, 1.0 and 1.2 mg/ml in 1.1, 3.2 and 5.3 M GdnCl respectively. This behavior is expected for solutions in thermodynamic equilibrium.

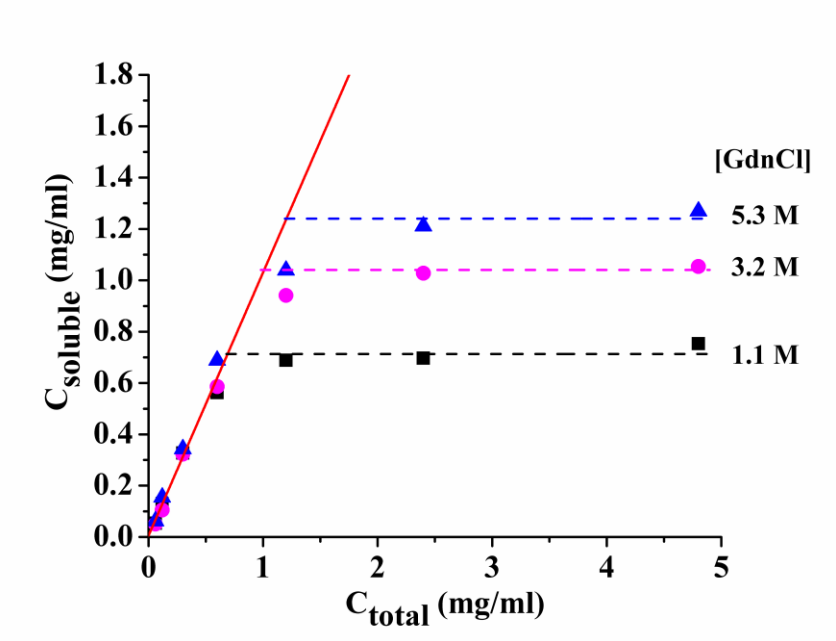

Figure S3. Soluble concentration ($C_{soluble}$) as a function of total concentration (C_{total}) of tyrosine measured in different concentrations of GdnCl. The solid red line corresponds to $C_{soluble} = C_{total}$ and the dotted lines are linear fit of the data for $C_{total} > C_{sat}$.

Relationship between $C_{soluble}$ and C_{total} for TMR-Aβ42 fibrils prepared with progressive seeding

The denaturant dependent apparent solubility data with progressively seeded amyloids (see Figure 6) and analysis of the data using equation 5 (see Figure 7D) indicate that the heterogeneity of the fibrils reduces progressively with successive seeding. We now examine if progressive seeding can give rise to purely homogeneous fibrils. To test this, we examine the relationship between soluble concentration and total concentration (i.e., $C_{soluble}$ vs. C_{total}) at 3 M GdnCl using TMR-Aβ42 amyloids prepared after 6^{th} generation of serial seeding. Figure S4 shows that $C_{soluble}$

increases linearly with C_{total} of the amyloids (i.e., $C_{soluble} \propto C_{total}$). This indicates that amyloids obtained even after 6th generation of seeding are not purely homogeneous.

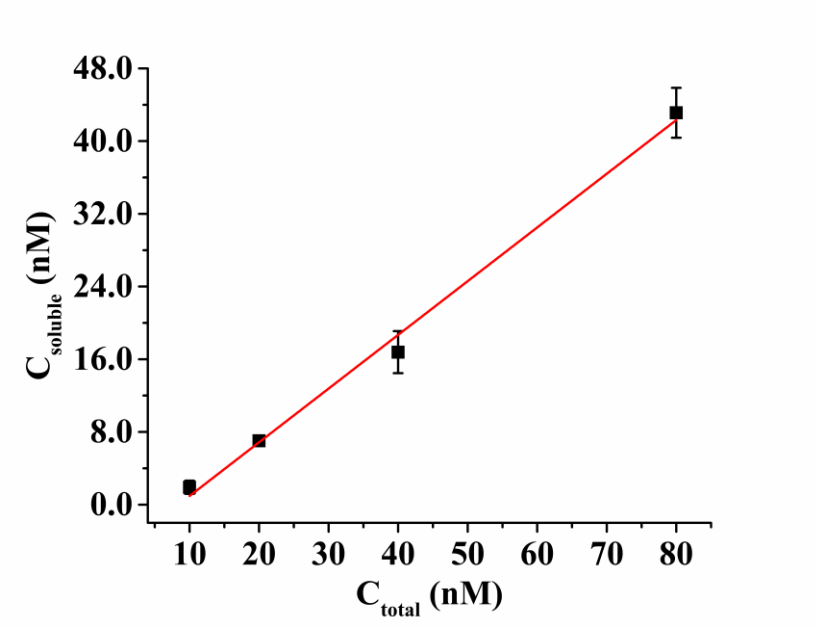

Figure S4. Soluble concentration as a function of total concentration of TMR-Aβ42 amyloids obtained after 6th generation of seeding. Aliquots (2, 4, 8 and 16 µl) of 6 µM stock of TMR-Aβ42 amyloids are diluted into PBS buffer containing 3 M GdnCl. Soluble concentrations of the amyloids are measured using fluorescence of TMR. Black squares represent the data and the solid red line is linear fit of the data.

Summary of the values of <ρ> and σ obtained from fitting of the denaturant dependent apparent solubility data using equation 5

Table S1 and S2 summarize the values of <ρ> and σ for amyloid aggregates obtained from analysis of the data presented in Figures 4A-C and 6 respectively using Eq. 5. The amyloids used for disaggregation have different preparation history, viz., different aggregation temperature, pH, ageing and with or without seeding. The distributions of ρ^* obtained are plotted in figure 7 in the manuscript. It may be seen from Table S1 that the mean (<ρ>) of the distributions increases with increasing temperature, pH, ageing indicating increase in stability. Table S2 shows that while the <ρ> remains the same, the standard deviation (σ) decreases with progressive seeding indicating decrease in heterogeneity of the amyloids.

Table S1: Mean kinetic stability (<ρ>) and heterogeneity (σ) of the amyloids obtained from analysis of the data presented in Figures 4A-C.

Figure no.	Temperature (^{0}C)	pH	Aging	< ρ> (M of GdnCl)	σ (M of GdnCl)
4A	25	7.4	2 days	3.42	1.87
4A	37	7.4	2 days	4.0	2.26
4B	37	7.4	24h	3.46	1.70
4B	37	5.7	24h	2.37	0.91
4C	37	7.4	2 days	2.6	1.42
4C	37	7.4	2 months	4.73	1.98
4C	37	7.4	4 months	6.73	3.12

Table S2: Effects of progressive seeding on mean kinetic stability (<ρ>) and heterogeneity (σ) of the amyloids obtained from analysis of the data presented in Figure 6.

No. of generations of serial seeding	< ρ> (M of GdnCl)	σ (M of GdnCl)
1	3.22±0.13	1.69±0.11
3	3.26±0.05	1.24±0.06
5	3.29±0.04	1.01±0.05

Reference:

1. Garai, K., and C. Frieden. 2013. Quantitative analysis of the time course of Aβ oligomerization and subsequent growth steps using tetramethylrhodamine-labeled Aβ. Proc. Natl. Acad. Sci. USA. 110:3321-3326.